Water Supply

Water Supply Vol 24 No 4, 1377 doi: 10.2166/ws.2024.049

Chloride ion sequestration by vetiver root biosorption: isotherm, kinetic, and thermodynamic analyses and ANN prediction

Riddhi Chandrakant Dhumal [a,*] and Parag Sadgir [b]

[a] Civil Engineering Department, College of Engineering, Pune, Maharashtra, India
[b] Civil Engineering Department, COEP Technological University, Pune, Maharashtra, India
*Corresponding author. E-mail: rcd21.civil@coeptech.ac.in

RCD, 0000-0001-8710-6593

ABSTRACT

The present research investigates the potential of activated vetiver root powder as a bioadsorbent for removing chloride ions from saline aqueous environments, especially relevant for addressing agricultural water scarcity. Factors such as pH, biomass dosage, contact duration, and initial salt ion concentration were examined. Thermodynamic analysis provided insights into the adsorption process, demonstrating the feasibility, non-spontaneous behavior, and exothermic nature of chloride ion adsorption onto activated vetiver root powder. The batch adsorption of chlorides adhered to the Langmuir equation and a pseudo-second-order kinetic model, demonstrating a monolayer adsorption capacity of 17.58 mg/g for activated vetiver powder. An artificial neural network (ANN) was used to develop a predictive model for estimating the percentage removal of chloride ions. The values of R^2 and mean squared error were used to determine the predictive performance of the ANN. In the near term, prospective commercial uses of activated vetiver powder merit further investigation through in-depth research using real wastewater containing salinity-inducing ion.

Key words: bioadsorbent, chloride ion removal, saline water, vetiver root powder, water quality

HIGHLIGHTS

- This study focused on vetiver root powder's efficacy in removing chloride ions under varied conditions.
- It explored the contrast between linear and nonlinear regression in isotherm and kinetics analyses.
- Thermodynamic assessment revealed a non-spontaneous and exothermic bioadsorption process.
- This study introduced an ANN model that predicts chloride ion removal, highlighting its potential in biosorption studies.

GRAPHICAL ABSTRACT

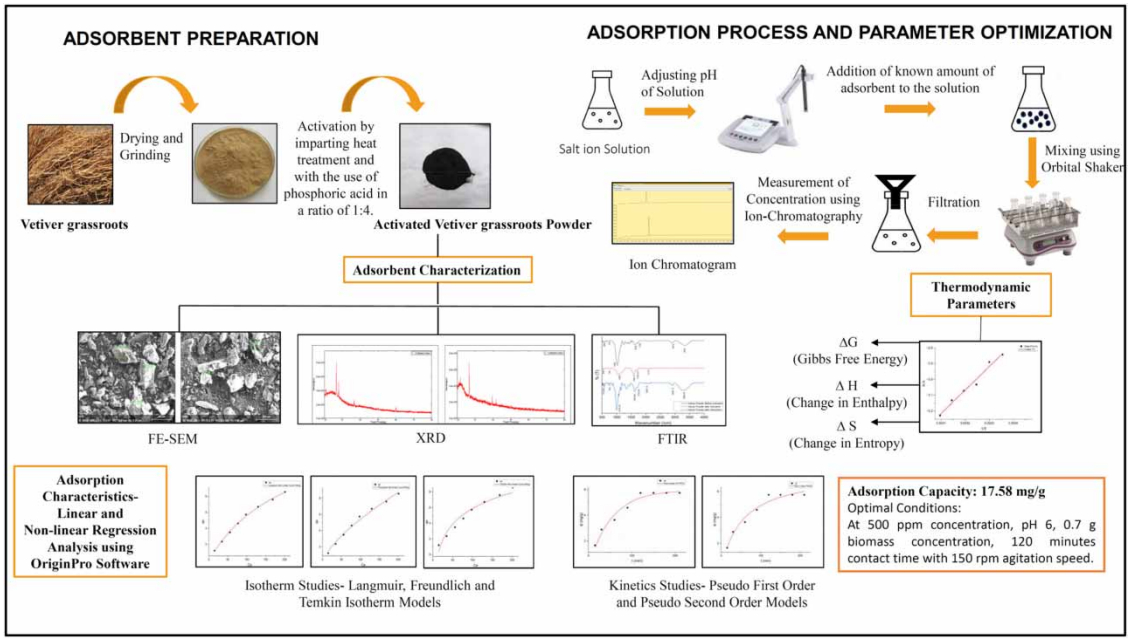

1. INTRODUCTION

Water scarcity, exacerbated by increasing salinity levels in surface and groundwater, poses a significant challenge to sustainable agricultural practices, notably in regions like India. Saline water, enriched with sodium chloride, adversely impacts plant growth. However, little research focuses on mitigating water salinity for irrigation purposes (Kaushal *et al.* 2021). Despite efforts to remediate soil salinity, minimal attention is devoted to decreasing salinity in saline water using organic amendments (Gunarathne *et al.* 2020).

Groundwater, which is a primary source of freshwater for various sectors, often contains high salt concentrations. This makes it unsuitable for irrigation and can have detrimental effects on soil conditions and ecosystems (Sharma & Bhattacharya 2017). The World Health Organization prescribes a chloride limit of 250 mg/L for drinking water purposes. The maximum permissible concentrations of chlorides in irrigation water, without causing yield losses, range from 350 to 1,750 ppm, depending on the cultivation of the crop (Thu *et al.* 2018). Saline water's impact on crop water absorption and the consequent risk of plant wilting, even when soil moisture further appears sufficient, further worsens agricultural challenges (Krishan *et al.* 2020).

While desalination technologies like reverse osmosis offer promise, their limitations – high costs, biofouling, and energy consumption – hinder widespread adoption (Sahu 2021). Alternative approaches using low-cost adsorbents, which are rich in organic compounds, have gained attention for their ability to remove ions that contribute to water salinity (Dhumal & Sadgir 2023). They are also being studied for their effectiveness in removing different pollutants from water (Nikhar *et al.* 2023) and their potential to contribute to sustainable water treatment approaches (Waikar & Sadgir 2023). Activated carbon, renowned for effective pollutant removal, especially from liquid phases, faces challenges like cost and process complexities (Saleem *et al.* 2019).

This study investigates vetiver biomass conversion into activated carbon to extract chloride ions from saline water, achieving a capacity of 17.58 mg/g at 600 °C pyrolysis. It delves into material characterization, process optimization, and kinetic evaluations. It also explores machine learning algorithms to forecast chloride ion removal rates. The aim is to establish vetiver root powder as a viable, cost-effective bioadsorbent for chloride ion elimination from saline water, particularly in agricultural applications.

2. MATERIALS AND METHODS

2.1. Adsorbent preparation

The adsorbents sourced in this research were collected, cleaned thoroughly with tap water, and then with deionized water to eliminate dust and dirt. The adsorbent was then dried in an air oven at 105°C for 5 h. Dried adsorbent was ground into powder using a mixer and sieved through a 180 μm sieve. The activation of vetiver root powder was accomplished by imparting heat treatment (at 600 °C) and with the use of phosphoric acid in a ratio of 1:4. The activated product was washed with water and dried, then stored in containers for the use in subsequent experiments (Harikumar *et al.* 2010).

2.2. Adsorbate preparation

A standard 500 ppm NaCl solution was prepared by dissolving 0.496 g of anhydrous sodium chloride in 1,000 mL of deionized water. The pH of the solution was adjusted with NaOH (0.1 M) or HCl (0.1 M) to the desired value. All chemicals used were of an analytical quality and were bought from local sources in Maharashtra, India.

2.3. Optimization of adsorption parameters

The preliminary part of this study was designed to optimize the parameters that influence the adsorption efficacy. This involved the outcome of pH variation (from 4 to 9), the dosage of adsorbent (from 1 to 10 g/L), contact time (from 15 to 210 min), and initial concentration C_0 of the adsorbate present in the solution. All experiments were accomplished in triplicate and in a constant volume of 100 mL prepared brackish water (dissolving NaCl in deionized water). The optimum settings were determined to examine the influence of the concentration of NaCl solution on the adsorption capacity of the bioadsorbent. The concentration tested range was in the range of 100–800 ppm. These tests were conducted after optimizing the functional pH, contact time, and adsorbent dosage.

Adsorption capacity (mg/g) and removal rate (RR%) were calculated using the following equations:

$$\text{Adsorption capacity (mg/g)} = \frac{(C_0 - C_e)\, V}{W} \times 100 \tag{1}$$

$$\text{RR \%} = \frac{C_0 - C_e}{C_0} \times 100. \tag{2}$$

where C_0 is the initial concentration of chloride ions in ppm, C_e is the remaining concentration of ions at equilibrium in ppm, W is the bioadsorbent mass in grams, and V is the volume of adsorbate in liters.

2.4. Characterization of adsorbent

The study extensively analyzed the physicochemical attributes of vetiver biomass to understand its fundamental properties and potential for interacting with metal ions. X-ray diffraction elucidated the biomass structure using Cu Kα radiation, scanning from 20° to 80° at a rate of 2° per minute. Fourier transform Infrared (FTIR) spectra identified functional groups interacting with chloride ions, covering the range of 400–4,000 cm^{-1} using an ATR-equipped Shimadzu IR affinity instrument. Additionally, the study assessed structural and textural properties like pore volume, diameter, and surface area via nitrogen adsorption/desorption isotherms at 77.35 K and conducted on a Quantachrome Novae 2200 Brunauer–Emmett–Teller (BET) surface area analyzer. These analyses yielded crucial insights into the porous nature and surface characteristics of the biomass, which contribute to our understanding of its adsorption capabilities.

2.5. Isotherm and kinetics modelling

In batch experiments, different chloride ion concentrations from 100 to 800 mg/L were studied to determine bioadsorption equilibrium through Temkin, Freundlich, and Langmuir models, as detailed in Table 1. Kinetic tests were conducted to establish equilibrium time, employing the pseudo-first-order and pseudo-second-order (PS2) models to investigate chloride ion adsorption onto vetiver powder, with equations outlined in Table 2.

Similarly, the governing equations for determining thermodynamic parameters like ΔH (change in enthalpy) and ΔG (Gibb's free energy) along with ΔS (change in entropy) for bioadsorption of the chloride ions utilizing activated vetiver

Table 1 | Isotherm model equation and parameters

Isotherm models	Equation	Parameters		R^2	RMSE	MSE	EABS	ARE	ERRSQ
Linear regression									
Langmuir	$C_e/q_e = 1/q_m K_L + C_e/q_m$	q_{max} (mg/g) a (l/mg)	14.76 0.004	0.997	0.005	0.024	0.031	0.159	0.168
Freundlich	$\ln q_e = \ln \mathrm{KF} + 1/n \ln C_e$	k (l/mg) n	0.162 0.75	0.992	0.007	0.0490	0.057	0.223	0.343
Temkin	$q_e = \mathrm{RT/bT} \ln(A_T) + \mathrm{RT/bT} \ln(C_e)$	A B	75.288 7.510	0.946	0.012	0.144	0.152	0.243	0.366
Non-linear regression									
Langmuir	$q_e = q_m K_L C_e/(1 + K_L C_e)$	q_{max} (mg/g) a (l/mg)	17.58 0.005	0.996	0.004	0.018	0.026	0.139	0.129
Freundlich	$q_e = K_f C_e \text{^} (1/n)$	k (l/mg) n	0.226 1.45	0.992	0.006	0.039	0.042	0.200	0.271
Temkin	$q_e = \mathrm{RT/bT} \ln (A_T{}^* C_e)$	A B	0.077 2.893	0.956	0.011	0.122	0.130	0.202	0.316

RMSE, root mean square error; MSE, mean square error; EABS, sum of the absolute errors; ARE, average relative error; ERRSQ, sum of squares of error; RT/bT is the Temkin constant related to heat of sorption (J/mol), A is the equilibrium binding constant corresponding to the maximum binding energy (L/g), R is the gas constant (8.314 J/mol K), and T is the absolute temperature (K).

Table 2 | Kinetics equations and model parameters

Kinetics model	Equation	Parameters		R^2	RMSE	MSE	EABS	ARE	ERRSQ
Linear regression									
PS1	$q_t = q_e(1 - e^{-k_1 t})$	Constant k_1 (/min) q_e cal (mg/g)	0.006 8.228	0.703	0.004	0.018	0.026	0.139	0.128
PS2	$q_t = q_e^2 k_2 t/(q_e k_2 t + 1)$	Constant k_2 (/min) q_e cal (mg/g)	0.019 6.728	0.9576	0.003	0.0099	0.014	0.095	0.069
Non-linear regression									
PS1	$q_t = q_e(1 - e^{-k_1 t})$	Constant k_1 (/min) q_e cal (mg/g)	0.020 7.359	0.9632	0.004	0.013	0.019	0.113	0.090
PS2	$q_t = q_e^2 k_2 t/(q_e k_2 t + 1)$	Constant k_2 (/min) q_e cal (mg/g)	0.020 5.960	0.98132	0.003	0.008	0.007	0.073	0.053

PS1, pseudo first order; PS2, pseudo second order

powder are listed below:

$$\Delta G = (-\mathrm{RT}) \ln K, \tag{3}$$

$$\Delta G = \Delta H - T\Delta S, \tag{4}$$

$$\ln K = (\Delta S/\mathrm{R}) - (\Delta H/\mathrm{RT}) \tag{5}$$

In the equation, ΔG represents Gibb's free energy (kJ/mol), Kf (Freundlich coefficient (L/Kg)), K stands for the adsorption distribution coefficient (g/L), q_e signifies the biosorption capacity at equilibrium (mg/g), C_e denotes the residual concentration of ions at equilibrium (g/L or mg/L), R denotes the universal gas constant (8.314 J/mol K), T represents the absolute temperature (K), ΔH indicates the change in enthalpy (kJ/mol), and ΔS signifies the change in entropy (J/mol K). Using experimental data, the Gibb's free energy (G) was calculated at various temperatures. The ln K vs. $1/T$ graph's slope and intercept were utilized to determine the enthalpy change (H) and entropy change (S) values. b is the Temkin constant related to heat of sorption (J/mol), and A is the equilibrium binding constant corresponding to the maximum binding energy (L/g).

2.6. Computational modeling

The application of machine learning methods to forecast the effectiveness of contaminant removal in hydrological streams continues to develop (Nguyen *et al.* 2022). However, due to a number of practical and financing limitations, this study aggregated batch adsorption trial data to evaluate artificial neural network (ANN) accuracy in predicting bioadsorbent performance for ion removal. The ANN architecture involves input and output layers, with an intermediate encoded layer. This layer is made up of nodes that are connected to form these layers. Nonlinear computations are made possible by activation functions such as sigmoid and rectified linear units (ReLU). The model employs a linear transfer function (purelin) and tansigmoid transfer function (tansig) within the encoded layer. The Levenberg–Marquardt algorithm is used for network training.

3. RESULTS AND DISCUSSION

3.1. Characterization of adsorbent

The displayed images (Figure 1) depict the surface characteristics of vetiver root powder both pre- and post-activation. Initially, the surface appeared smooth with a hard and dense structure, lacking any porous formations. Examination via scanning electron microscopy (SEM) revealed an absence of uniformity in particle size and shape. Conversely, the activated vetiver root powder showcased an irregular surface with a well-defined pore structure post-treatment. This transformation indicated a substantial impact of the phosphoric acid activation process in inducing the formation of porous structures on the surface.

The X-ray diffraction (XRD) analysis of vetiver root powder (Figure 2) reveals distinctive characteristics pre- and post-activation. In the initial state, the spectrum showcases prominent diffraction peaks, signifying a primarily crystalline structure.

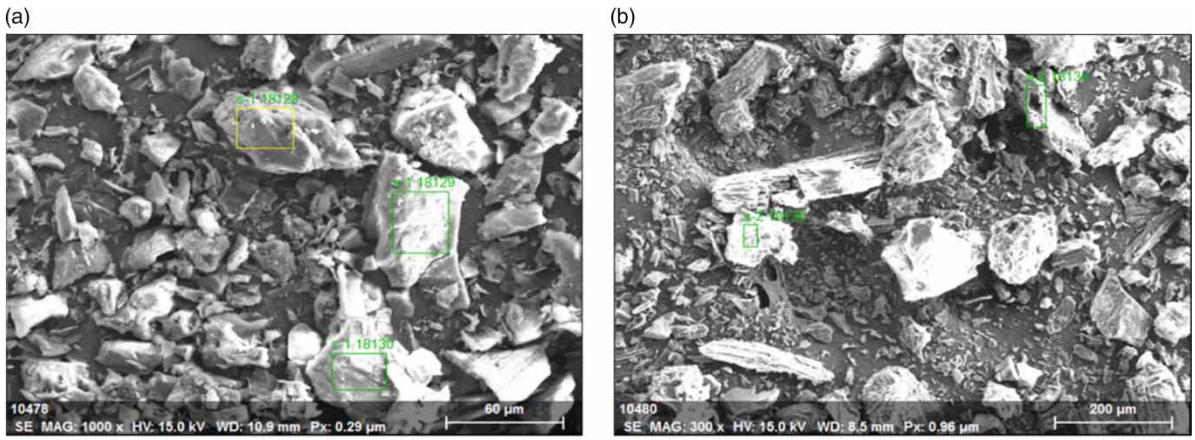

Figure 1 | SEM analysis of the vetiver powder before (a) and after (b) activation.

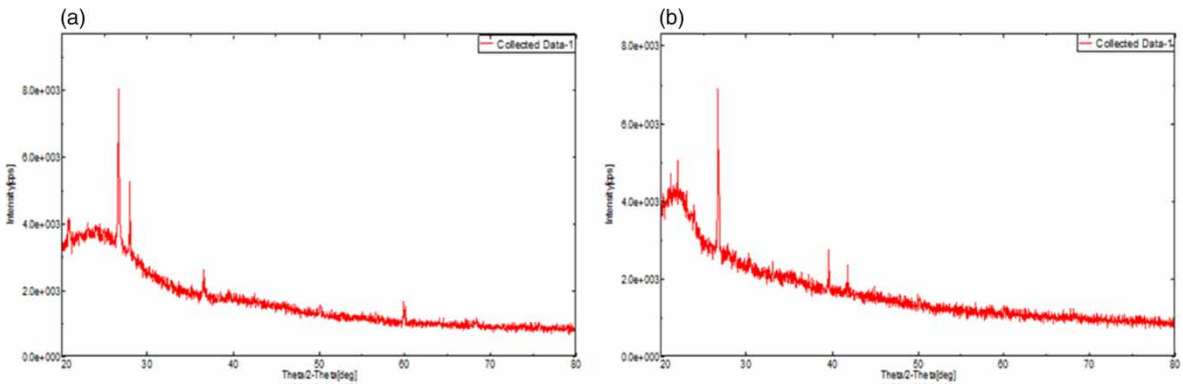

Figure 2 | XRD images of the vetiver powder before (a) and after (b) activation.

Notably, there is a dominant peak centered at 2θ values of 20.85° and approximately 26.70°, indicating an augmented regularity in the crystalline arrangement. Further examination of the XRD pattern demonstrates specific diffraction angles, including 20.85°, 27.9°, 36.60°, and 59.91°, correlating to crystal planes (311), (420), (422), and (951), respectively, as per JCPDS 81-2220. Interestingly, in the pre-activation stage, distinct peaks around 2θ of approximately 26.76° are observed, indicating the presence of graphite-like diffraction patterns. However, the resolution between these peaks is compromised due to the semi-crystalline nature of cellulose (Rong *et al.* 2001). However, in the post-activation, these peaks exhibit higher intensity compared to the pre-activation state. This heightened intensity might be attributed to an enhancement in crystallinity post-activation, potentially due to the elimination of certain binding materials during the activation process.

FTIR spectra, in a region of 4,000–500 cm^{-1}, of the vetiver root powder before and after activation along with after adsorption are shown in Figure 3. The peaks extricated from FTIR spectra are given in Table 3. The frequency at 1,725–1,702 cm^{-1} was derived from the carboxyl (C = O) vibration of hemicellulose. The major peaks are observed in all three spectra, as shown

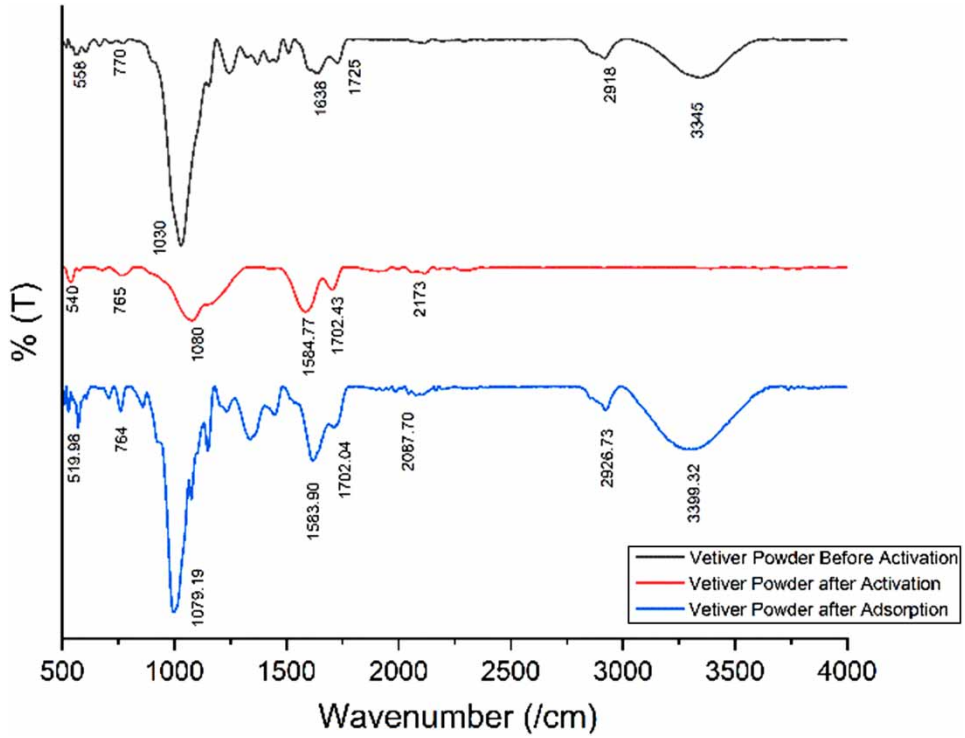

Figure 3 | FTIR spectra of vetiver powder before and after activation and after adsorption.

Table 3 | FTIR peaks and tentative assignments

FTIR peak	Assigned functional group	Band wavenumber (cm^{-1})		
		Vetiver root powder before activation	Vetiver root powder after activation	Activated vetiver root powder after adsorption
1	(O–H) Hydroxyl	3,345	–	3,399.32
2	(C–H) Methyl	2,918	2,173	2,087.70
3	(C = O) Carboxyl	1,725	1,702.43	1,702.04
4	(C = C) Alkene	1,638	1,584.77	1,583.90
5	(C–O) Phenolic, (C–OH) Ethers	1,030	1,080	1,079.19
6	(C–H) and ($CH = CH_2$) Aromatic structures	770–558	765–540	764–519.98

in Figure 3. C–O, O–H, C = O, and C = C functional groups tended to be enmeshed in the course of the bioadsorption of chloride ions onto activated vetiver root powder. Moreover, after activation of the vetiver powder, the peak at ~3,345 is no longer present due to the thermal treatment it undergoes; however, the presence of the hydroxyl group can be found again in the FTIR spectra of the vetiver powder after adsorption. This is because the adsorption process leads to a chemical change.

Vetiver root powder's surface area and pore properties can be identified by applying BET (Table 4) analysis to compute the pore size and surface area and the Barrett–Joiner–Halenda procedure for estimating the pore volume. Before the N_2 adsorption experiment, the vetiver root powder samples are degassed at 120 °C for 6 h in order to measure the surface area and remove any adsorbed species. Nitrogen adsorption isotherms, performed at an adsorption temperature of 77.35 K, provide information on the textural characteristics of vetiver root powder that has been pre- and post-activated. These isotherms are included in Table 4. Based on analysis, the material is classified as mesoporous by the IUPAC with a pore size of 3.4 nm. It has been shown that this mesoporous quality promotes enhanced dispersion of particles (Fatombi *et al.* 2019; Rosanti *et al.* 2022).

3.2. Optimization of parameters

3.2.1. Effect of pH

In the study, pH fluctuations between 4 and 9 were investigated. This range was determined to be commensurate with the sensitivity of the ion chromatography (IC) column. There was a notable improvement in the absorption of chloride ions, ranging from 60.2 to 75.85%, when the pH was raised from 4 to 6. This finding suggests that a higher pH fosters the adsorption process, resulting in a greater adsorption balance. As a result, within this pH range, the amount of chloride ions adsorbed, q_e, increased significantly, increasing from 6.02 to 7.58 mg/g, as shown in Figure 4. This behavior is attributed to the adsorbent's surface charge becoming more positively charged as the pH increases. This change promotes stronger columbic interactions between chloride ions and the adsorbent's surface, facilitating greater adsorption (Kumar & Yadav 2007).

However, when pH levels exceed 6 and move toward the alkaline end of the spectrum, reaching up to 9. In this instance, the pH rise did not result in a corresponding rise in chloride ion absorption. Instead, the removal rate dropped from 75 to 71%, suggesting a subsequent decline in adsorption capacity. Chloride ions and hydroxyl ions compete for adsorption locations on the exterior of the adsorbent, which is the cause of this decline. The concentration of hydroxyl ions rises as the pH becomes more alkaline. This increase effectively competes with chloride ions for binding sites, resulting in a decrease in the total adsorption of chloride ions (Harikumar *et al.* 2010).

3.2.2. Effect of adsorbent dosage

The graph in Figure 5 shows the progression of chloride elimination at a neutral pH of 7. The chloride removal rate steadily increased as the adsorbent quantity was upraised from 1 to 7 g/L. The removal rate increased from the initial level of 59 to 80%. The expansion of the accessible surface area and the activation of extra adsorption sites on the exterior of adsorbent material provided a larger surface area, increasing the potential for chloride ions to interact with active sites of adsorption.

Increasing the adsorbent amount from 7 to 10 g/L showed a plateau in chloride adsorption, indicating that beyond a certain point, additional material did not significantly enhance adsorption capacity. This suggests a loss of significance in chloride removal rates with higher adsorbent dosages. The larger dose had a negative impact on adsorption capacity due to diffusional constraints and a reduced solvent ratio. This resulted in a slower approach and binding of chloride ions to

Table 4 | Textural properties of vetiver powder pre- and post-activation

Particulars	Pre-activation vetiver root powder	Post-activation vetiver root powder
Surface area BET N_2 (m^2/g)	11.809	645.175
Volume of pore (cc/g)	0.011	0.212
Diameter of pore (nm)	3.428	3.407
Width of pore (nm)	5.880	2.107
Size of particle (μm)	0.755	0.454

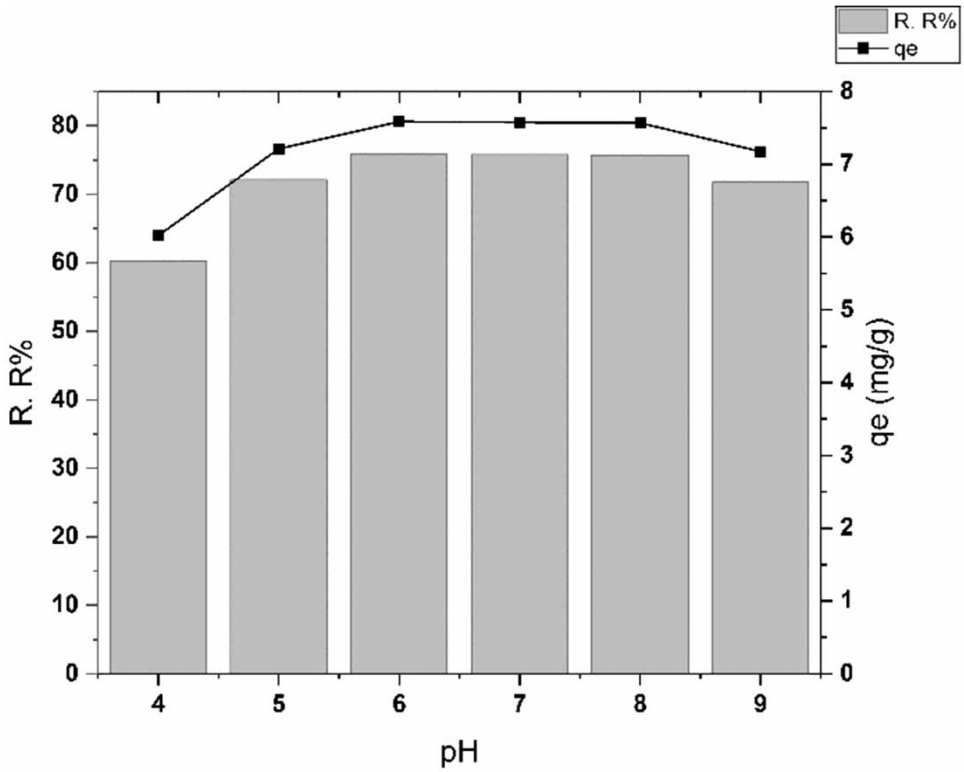

Figure 4 | Effect of pH on the removal rate of chloride using activated vetiver root powder.

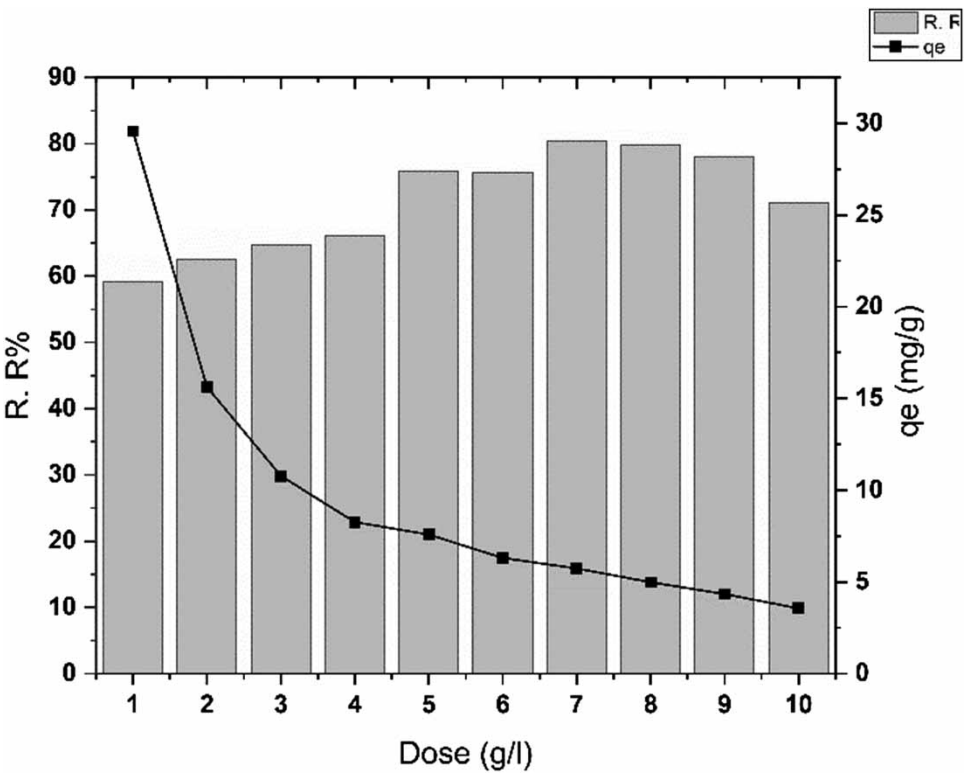

Figure 5 | Effect of adsorbent dosage on the removal rate of chloride using activated vetiver root powder.

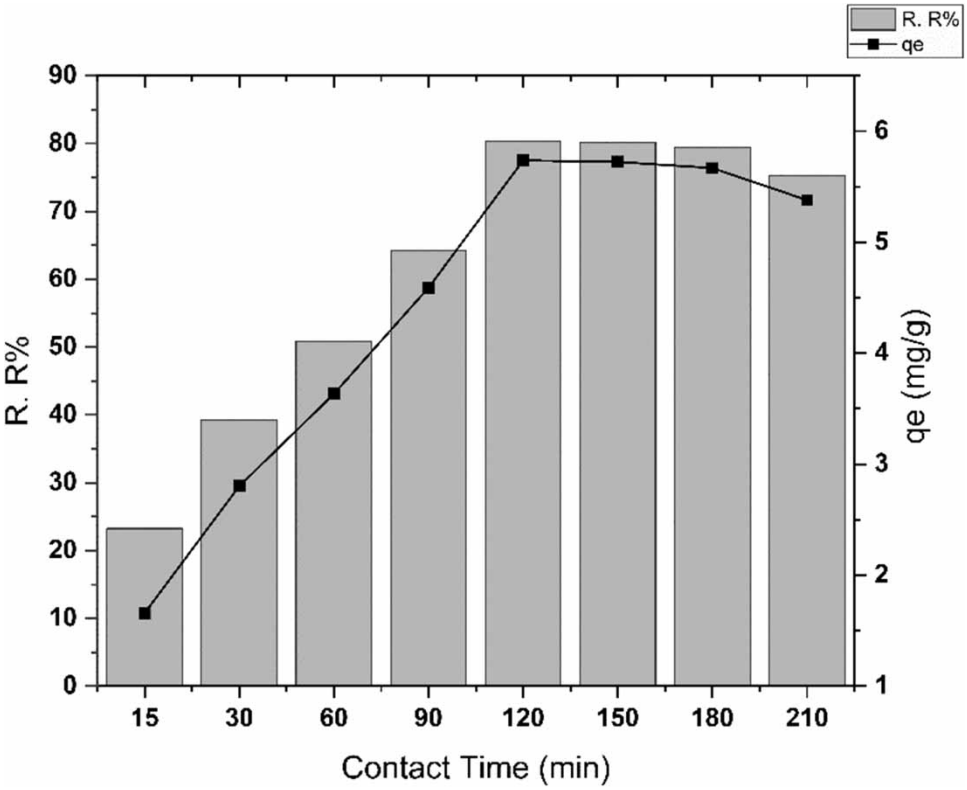

Figure 6 | Effect of contact time on the removal rate of chloride using activated vetiver root powder.

active adsorption sites. Consequently, the concentration gradient driving ion diffusion diminished, hindering the efficacy of higher adsorbent doses (Jagtap *et al.* 2011; Shahawy *et al.* 2021).

3.2.3. Effect of contact time

The affiliation of contact time with chloride removal rates, alongside adsorption capacity (q_e), is pivotal in understanding bioadsorption processes. Figure 6 illustrates a substantial increase in chloride removal, rising from 23.2 to 80.3% as the contact time increased from 15 to 120 min. This notable enhancement in removal efficiency underscores the significance of initial contact time in facilitating chloride adsorption, which is primarily attributed to the accessibility of effective binding locations on the bioadsorbent material.

Concurrently, the adsorption capacity (q_e) reached 5.73 mg/g after 120 min, indicating the amount of chloride ions adsorbed per unit amount of the bioadsorbent. However, the plateauing of chloride elimination and q_e beyond 120 min suggests an equilibrium or saturation point, where further contact time does not significantly increase chloride adsorption (Zhang *et al.* 2017). This pattern aligns with previous studies (Jiang *et al.* 2016) that observed optimal efficacy in the early contact phases due to the availability of open surfaces for bioadsorption, followed by a saturation of active binding sites leading to declining removal rates over extended contact periods.

3.2.4. Effect of initial concentration

The influence of the initial concentration of Cl^- was assessed in the 100–800 mg/L range under the pre-optimized parameters, i.e., pH = 6, a contact period of 120 min, and a 7 g/L adsorbent dose. As shown in Figure 7, depending on the initial concentration of each batch, a rise in the initial chloride level from 100 to 800 mg/L caused a reduction in the percentage of the chloride removal rate from 85 to 74.8%. Q_e increased from 1.21 to 8.55 mg/g in the meanwhile. A consistent quantity of adsorbent leads to heightened chloride levels in the solution with elevated preliminary concentrations, consequently enhancing the binding capacity of the adsorbent for chloride (Bayu *et al.* 2022). A substantial mass transfer

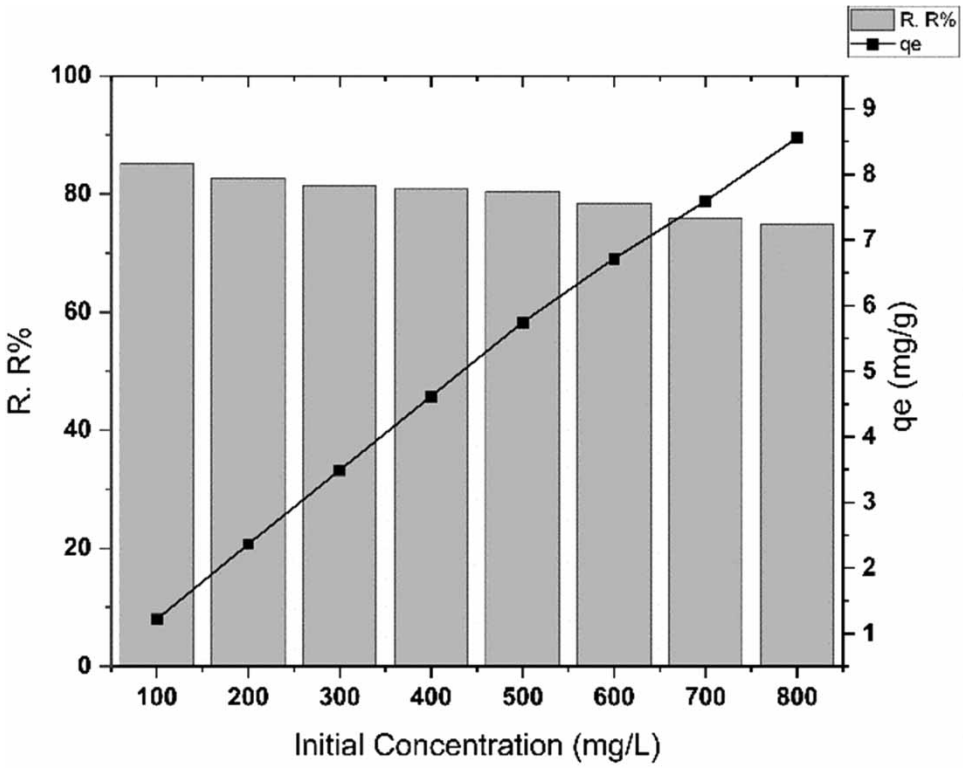

Figure 7 | Effect of initial concentration of adsorbate on the removal rate of chloride using activated vetiver root powder.

driving force is the cause of the increase in adsorption with the rise in chlorides. This is due to the fact that a larger starting chloride ion concentration enhances the concentration gradient's driving force (Askari *et al.* 2023).

3.3. Adsorption isotherms

Adsorption isotherms portray a crucial role in understanding how adsorbate molecules distribute between liquid and solid phases, shedding light on adsorption mechanisms and surface characteristics of adsorbents. Langmuir, Freundlich, and Temkin isotherms were employed in this study (Figures 8 and 9) to analyze data from adsorption trials. Both linearization and nonlinear regression methods were used to derive isotherm parameters, detailed in Table 1, enabling a comprehensive assessment of their effectiveness in describing chloride ion adsorption onto activated vetiver powder.

The Langmuir isotherm emerged as the most suitable model for explaining Cl^- ion adsorption due to its stronger correlation coefficient (R^2) compared to the Freundlich model. Supported by lower error values and substantial R^2 values, the Langmuir isotherm confirmed its applicability through nonlinear regression. It indicated that there was a monolayer adsorption of chloride ions onto activated vetiver powder with a maximum adsorption capacity (q_{max}) of 17.58 mg/g (Ayawei *et al.* 2017). Conversely, the Freundlich isotherm exhibited lower correlation coefficients, typically relevant to heterogeneous surfaces, although the 'n' value suggested relatively strong adsorption of chloride ions on the exterior of adsorbent (Kumar *et al.* 2019).

The Langmuir isotherm's superiority was reinforced by improved nonlinear regression performance, confirming its validity in representing chloride ion bioadsorption onto activated vetiver powder. The Temkin isotherm, on the other hand, was found to be inadequate in describing chloride ion adsorption onto activated vetiver powder, as evidenced by residual plots, coefficient of determination (R^2) values, and errors shown in Table 1.

3.4. Kinetics modelling

The study assessed kinetic models using both linear and nonlinear regression methods through OriginPro 2023b software. These models were systematically aligned with experimental data on chloride ion bioadsorption kinetics (Figures 10

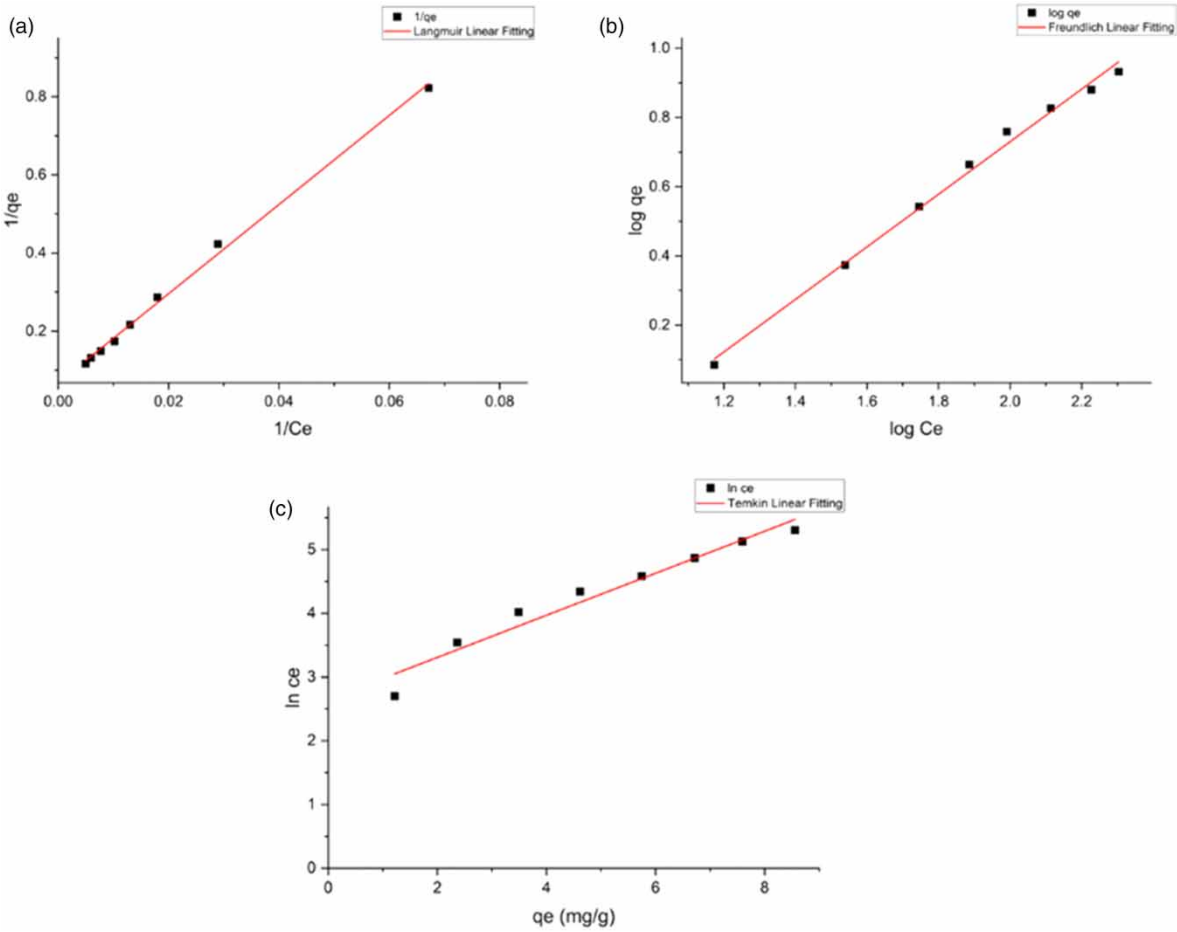

Figure 8 | Bioadsorption isotherm linear model fitted by Langmuir (a), Freundlich (b), and Temkin (c).

and 11), and the resulting parameters are compiled in Table 2. The evaluation, which indicated R^2 values exceeding 0.98 for the pseudo-second-order model through nonlinear regression, underlined its strong concordance with experimental data.

Additionally, the root mean square error (RMSE) values robustly supported the pseudo-second-order model's close fit to the experimental findings, affirming its superior performance in both linear and nonlinear regression analyses. Across all observations, the nonlinear versions of kinetic models consistently outperformed their linear counterparts. This was evident in the higher R^2 values and lower RMSE values, which signify enhanced accuracy in characterizing bioadsorption kinetics.

In summary, the study found the pseudo-second-order model to be highly effective in explaining chloride ion bioadsorption onto vetiver powder. With superior R^2 values, low RMSE values, and consistent performance in both linear and nonlinear regression analyses, the PS2 model emerged as the most suitable choice for accurately depicting bioadsorption kinetics, as presented in Table 2.

3.5. Thermodynamic parameters

Table 5 outlines the derived thermodynamic parameters, i.e., ΔG (Gibb's free energy), ΔH (change in enthalpy), and ΔS (change in entropy) for chloride ion bioadsorption with activated vetiver powder. Additionally, Figure 12 illustrates the graph of ln K versus $1/T$ for the activated vetiver powder.

The positive ΔG values confirm the feasibility of chloride ion bioadsorption onto activated vetiver powder, denoting a non-spontaneous reaction. The negative ΔH signifies an exothermic interaction between chloride ions and vetiver powder, while

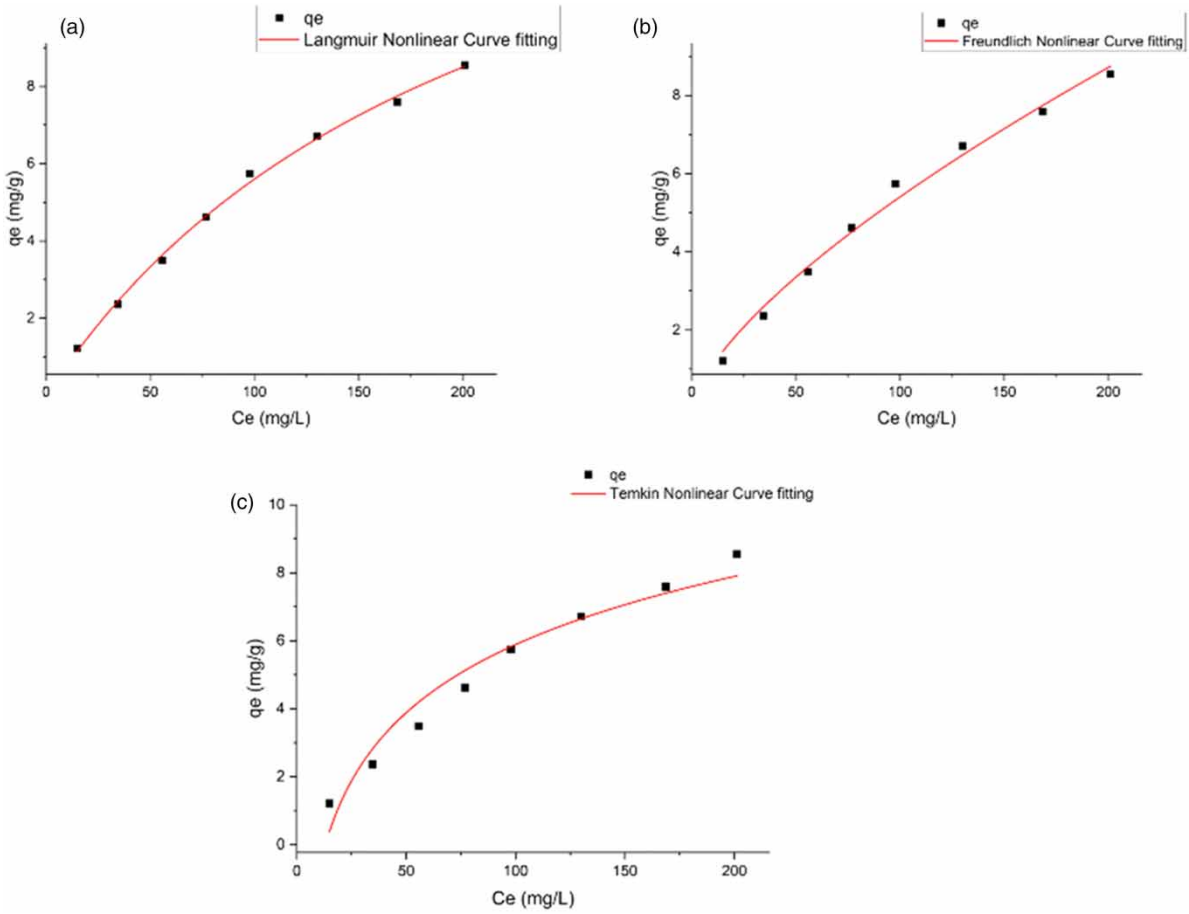

Figure 9 | Bioadsorption isotherm nonlinear model fitted by Langmuir (a), Freundlich (b), and Temkin (c).

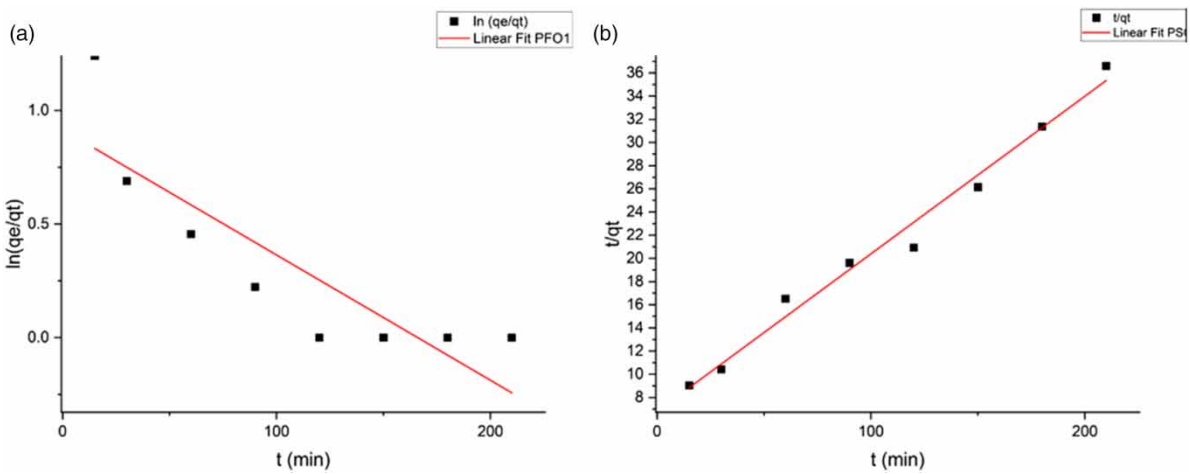

Figure 10 | Bioadsorption kinetics model of chloride ions on activated vetiver powder – linear (a) pseudo-first-order and (b) pseudo-second-order.

the negative ΔS indicates decreased uncertainty at the solid–liquid interface, suggesting increased orderliness in the course of adsorption. These negative estimates for ΔH and ΔS collectively imply a predominantly physical adsorption process without substantial structural changes in the adsorbent material (Ebelegi *et al.* 2020; Paranjape & Sadgir 2023).

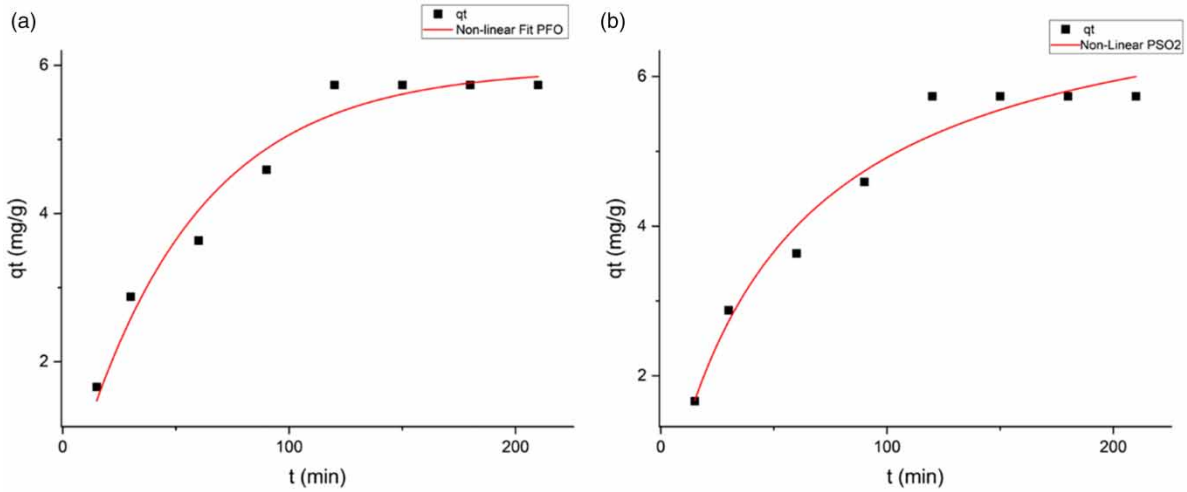

Figure 11 | Bioadsorption kinetics model of chloride ions on activated vetiver powder – non-linear (a) pseudo-first-order and (b) pseudo-second-order.

Table 5 | Thermodynamics parameters for the adsorption of chloride ions onto activated vetiver root powder

Biomass	*t* (K)	Δ*G* (kJ/mol)	Δ*H* (kJ/mol)	Δ*S* (kJ/mol K)
Activated vetiver powder	298	7.0269	– 12.3642	– 0.0651
	303	7.3523		
	308	7.6776		
	313	8.0030		
	318	8.3283		
	323	8.6537		

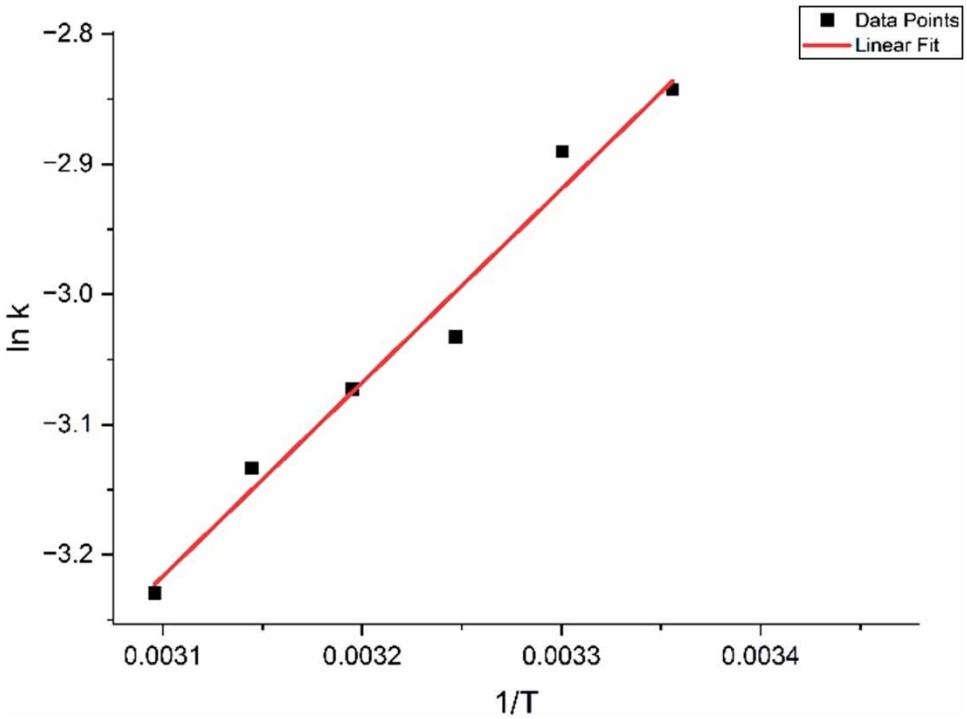

Figure 12 | Thermodynamic plot for the adsorption of chloride ions by activated vetiver root powder.

3.6. Computation modelling

This study developed an ANN model with two layers to assess chloride ion biosorption by activated vetiver powder. The comprehensive model details are presented in Table 6. Splitting the data into training, validation, and test subsets, 85% was used for training and 15% for testing the model's predictive capacity for new data points. This allowed us to evaluate the ANN model's general performance.

Multiple feedforward networks were trained to determine the optimal architecture by minimizing the mean squared error (MSE). The preferred configuration of the ANN model consisted of two hidden layers (10 neurons each), an output layer (one neuron), and a feedforward neural network with an input number of seven. This configuration is denoted as MLP (7:10:1:1) for inputs, hidden layers, output layer, and output, respectively. Utilizing the Levenberg–Marquardt algorithm, this network was trained to establish ideal weights and biases.

Figure 13(a) illustrates the goodness of fit of the anticipated performance of the ANN model to the experimental output. The reliability of the generated ANN model can be observed by its correlation coefficient of 0.992. Overall predictive precision for the model was concluded to be 99% through the procedure of validation (Figure 13(b)). On different data that were not used to train the model, the precision of the proposed neural network models for the percentage of chloride ion removal was also assessed, and noted R^2 was 0.9754 (Figure 13(c)).

Table 6 | ANN architecture, parameters, and performance

ANN architecture	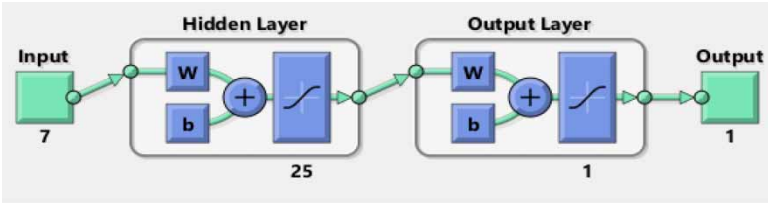
Input parameters	pH, contact time (min), bioadsorbent dose (g/L), agitation speed (rpm), temperature (°C), initial metal ion concentration (mg/L), adsorption capacity (mg/g), removal efficiency (%)
No. of layers	2
No. of neurons	1–10
Training algorithm	Levenberg–Marquardt (trainlm)
Transfer function	Logsig
Max epochs	1,000
Training data and testing data	85%, 15%
R^2	0.99

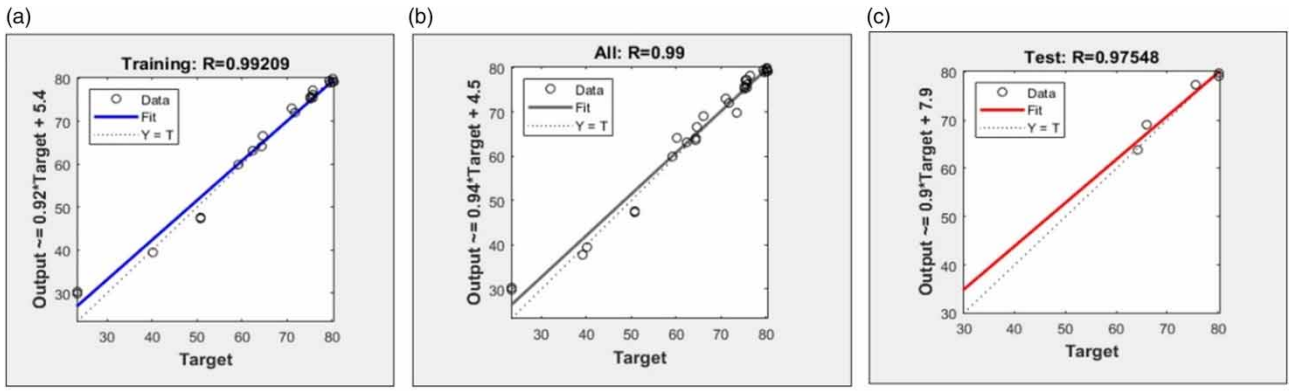

Figure 13 | Scatter plot for ANN indicating efficiency – (a) during training, (b) overall, and (c) during testing.

4. CONCLUSION

Activated vetiver grass root powder proves to be an environmentally sustainable and economically viable biosorbent for chloride ion extraction from saline media, demonstrating a maximum bioadsorption potential of 17.58 mg/g under optimized conditions. The Langmuir model effectively captured this process, establishing optimal parameters at 500 ppm concentration, pH 6, 0.7 g of biomass concentration, 120 min contact time with 150 rpm agitation speed.

Using nonlinear regression, the study validated ideal isotherms and kinetics with the pseudo-second-order model for kinetics and the Langmuir model for adsorption. Thermodynamic analysis revealed the feasibility, non-spontaneous nature, and exothermicity of chloride ion adsorption onto activated vetiver root powder, offering insights into the process.

Leveraging machine learning, specifically the ANN, enabled precise predictions of chloride ion extraction from saline solutions. These predictions exhibit strong alignment with experimental results, promising efficient bioadsorption predictions, and significant time and cost-savings. This incorporation of machine learning represents a pivotal stride in understanding bioadsorption processes, potentially revolutionizing environmental engineering practices for water and wastewater treatments.

Activating vetiver root powder provides a sustainable approach to reduce agricultural waste while creating valuable adsorbents, enhancing water quality specifically for irrigation purposes. Future research avenues should focus on enhancing or modifying the biomass for enhanced removal rates of chlorides. Examining activated vetiver biomass within intricate systems containing various co-ions in wastewater effluents is suggested to comprehensively assess its bioadsorptive traits. Moreover, exploring column studies, advancing pilot-scale commercialization, exploring adsorbent desorption and reuse, and formulating secure disposal approaches for the laden adsorbent would enhance and broaden this research domain.

ACKNOWLEDGEMENTS

The authors extend their sincere gratitude to COEP Technological University, Pune for their invaluable support and resources provided throughout this research endeavor.

AUTHOR CONTRIBUTIONS

R.C. Dhumal and P. Sadgir conceptualized the whole article and developed the methodology. R.C. Dhumal performed the experimentation and presented the data for the first draft of the manuscript. P. Sadgir provided guidance and reviewed the manuscript. All authors read and approved the final manuscript.

DATA AVAILABILITY STATEMENT

All relevant data are included in the paper or its Supplementary Information.

CONFLICT OF INTEREST

The authors declare there is no conflict.

REFERENCES

Askari, R., Mohammadi, F., Moharrami, A., Afshin, S., Rashtbari, Y., Vosoughi, M. & Dargahi, A. 2023 Synthesis of activated carbon from cherry tree waste and its application in removing cationic red 14 dye from aqueous environments. *Appl. Water Sci.* **13**. https://doi.org/10.1007/s13201-023-01899-1.

Ayawei, N., Ebelegi, A. N. & Wankasi, D. 2017 Modelling and interpretation of adsorption isotherms. *J. Chem.* https://doi.org/10.1155/2017/3039817.

Bayu, K., Geremew, A., Deriba, W., Mulugeta, Y., Wagari, S. & Dirirsa, G. 2022 Fluoride removal efficiency of Tulsi (*Ocimum sanctum*) from water. *Water Supply* **22**, 496–509. https://doi.org/10.2166/ws.2021.257.

Dhumal, R. & Sadgir, P. 2023 Bioadsorbents for the removal of salt ions from saline water: A comprehensive review. *J. Eng. Appl. Sci.* https://doi.org/10.1186/s44147-023-00253-1.

Ebelegi, A. N., Ayawei, N. & Wankasi, D. 2020 Interpretation of adsorption thermodynamics and kinetics. *Open J. Phys. Chem.* **10**, 166–182. https://doi.org/10.4236/ojpc.2020.103010.

Fatombi, J. K., Osseni, S. A., Idohou, E. A., Agani, I., Neumeyer, D., Verelst, M., Mauricot, R. & Aminou, T. 2019 Characterization and application of alkali-soluble polysaccharide of *Carica papaya* seeds for removal of indigo carmine and Congo red dyes from single and binary solutions. *J. Environ. Chem. Eng.* **7**. https://doi.org/10.1016/j.jece.2019.103343.

Gunarathne, V., Senadeera, A., Gunarathne, U., Biswas, J. K., Almaroai, Y. A. & Vithanage, M. 2020 Potential of biochar and organic amendments for reclamation of coastal acidic-salt affected soil. *Biochar* **2**, 107–120. https://doi.org/10.1007/s42773-020-00036-4.

Harikumar, P. S. P., Jaseela, C. & Megha, T. 2010 Defluoridation of water using bioadsorbents. *Pollut. Res.* **29**, 707–711. https://doi.org/10.4236/ns.2012.44035.

Jagtap, S., Yenkie, M. K., Das, S. & Rayalu, S. 2011 Synthesis and characterization of lanthanum impregnated chitosan flakes for fluoride removal in water. *Desalination* **273**, 267–275. https://doi.org/10.1016/j.desal.2010.12.032.

Jiang, Z., Cao, B., Su, G., Lu, Y., Zhao, J., Shan, D., Zhang, X., Wang, Z. & Zhang, Y. 2016 Comparison on the surface structure properties along with Fe(II) and Mn(II) removal characteristics of rice husk ash, inactive *Saccharomyces cerevisiae* powder, and rice husk. *Biomed. Res. Int.* **2016**, 7183951. https://doi.org/10.1155/2016/7183951.

Kaushal, S. S., Likens, G. E., Pace, M. L., Reimer, J. E., Maas, C. M., Galella, J. G., Utz, R. M., Duan, S., Kryger, J. R., Yaculak, A. M., Boger, W. L., Bailey, N. W., Haq, S., Wood, K. L., Wessel, B. M., Park, C. E., Collison, D. C., Aisin, B. Y., ʻaaqob, I., Gedeon, T. M., Chaudhary, S. K., Widmer, J., Blackwood, C. R., Bolster, C. M., Devilbiss, M. L., Garrison, D. L., Halevi, S., Kese, G. Q., Quach, E. K., Rogelio, C. M. P., Tan, M. L., Wald, H. J. S. & Woglo, S. A. 2021 Freshwater salinization syndrome: From emerging global problem to managing risks. *Biogeochemistry* **154**, 255–292. https://doi.org/10.1007/s10533-021-00784-w.

Krishan, G., Bisht, Ghosh, N. C. & Prasad, G., 2020 Water Science and Technology Library Environmental Processes and Management Tools and Practices, pp. 361–380. https://doi.org/10.1007/978-3-030-38152-3_19.

Kumar, S. & Yadav, J. P. 2007 Fluoride removal by mixtures of activated carbon prepared from Neem (*Azadirachta indica*) and Kikar (*Acacia arabica*) leaves. *Article Indian J. Chem. Technol.* **14**, 355–361.

Kumar, K. V., Gadipelli, S., Wood, B., Ramisetty, K. A., Stewart, A. A., Howard, C. A., Brett, D. J. L. & Rodriguez-Reinoso, F. 2019 Characterization of the adsorption site energies and heterogeneous surfaces of porous materials. *J. Mater. Chem. A Mater.* https://doi.org/10.1039/c9ta00287a.

Nguyen, X. C., Ly, Q. V., Nguyen, T. T. H., Ngo, H. T. T., Hu, Y. & Zhang, Z. 2022 Potential application of machine learning for exploring adsorption mechanisms of pharmaceuticals onto biochars. *Chemosphere* **287**. https://doi.org/10.1016/j.chemosphere.2021.132203.

Nikhar, C. K., Vyas, G. S. & Dalvi, R. S. 2023 Unlocking the potential of adsorption in distillery wastewater treatment: A comprehensive review. *Water Conserv. Sci. Eng.* **8**, 1–16.

Paranjape, P. & Sadgir, P. 2023 Linear and nonlinear regression methods for isotherm and kinetic modelling of iron ions bioadsorption *using Ocimum sanctum* Linn. leaves from aqueous solution. *Water Pract. Technol.* **18**, 1807–1827. https://doi.org/10.2166/wpt.2023.110.

Rong, M. Z., Zhang, M. Q., Liu, Y., Yang, G. C. & Zeng, H. M. 2001 The effect of fiber treatment on the mechanical properties of unidirectional sisal-reinforced epoxy composites. *Compos. Sci. Technol.* **61**, 1437–1447.

Rosanti, A. D., Kusumawati, Y., Hidayat, F., Fadlan, A., Wardani, A. R. K. & Anggraeni, H. A. 2022 Adsorption of methylene blue and methyl orange from aqueous solution using Orange Peel and CTAB-modified orange peel. *J. Turk. Chem. Soc.* A Chem. **9**, 237–246. https://doi.org/10.18596/jotcsa.1003132.

Sahu, P. 2021 A comprehensive review of saline effluent disposal and treatment: Conventional practices, emerging technologies, and future potential. *J. Water Reuse Desalination* **11**, 33–65. https://doi.org/10.2166/wrd.2020.065.

Saleem, J., Bin Shahid, U., Hijab, M., Mackey, H. & McKay, G. 2019 Production and applications of activated carbons as adsorbents from olive stones. *Biomass. Convers. Biorefin.* **9**, 775–802. https://doi.org/10.1007/s13399-019-00473-7/Published.

Shahawy, A. E., Ahmed, I. A., Wagdy, R., Ragab, A. H. & Shalaby, N. H. 2021 *Phragmites australis* (Reed) as an efficient, eco-friendly adsorbent for brackish water pre-treatment in reverse osmosis: A kinetic study. *Molecules* **26**(19), 6016. https://doi.org/10.3390/molecules26196016.

Sharma, S. & Bhattacharya, A. 2017 Drinking water contamination and treatment techniques. *Appl. Water Sci.* **7**, 1043–1067. https://doi.org/10.1007/s13201-016-0455-7.

Thu, T. T. P., Hideshi, Y. & Takeo, Y. 2018 Allocation of macronutrients in roots, sheaths, and leaves determines salt tolerance in rice. *Am. J. Plant Sci.* **09**, 1051–1069. https://doi.org/10.4236/ajps.2018.95081.

Waikar, M. & Sadgir, P. 2023 Sustainable development in circular economy: A review. In: *Lecture Notes in Civil Engineering*. Springer Science and Business Media Deutschland GmbH, pp. 629–639. https://doi.org/10.1007/978-981-19-2145-2_48.

Zhang, X., Hao, Y., Wang, X. & Chen, Z. 2017 Rapid removal of zinc(II) from aqueous solutions using a mesoporous activated carbon prepared from agricultural waste. *Materials* **10**(9), 1002. https://doi.org/10.3390/ma10091002.

First received 11 January 2024; accepted in revised form 2 March 2024. Available online 15 March 2024